ARTICLES

$\pi N \to \eta N$ and $\eta N \to \eta N$ partial-wave T matrices in a coupled, three-channel model

Mijo Batinić, Ivo Šlaus, and Alfred Švarc
Rudjer Bošković Institute, 41001 Zagreb, Croatia

B.M.K. Nefkens
University of California Los Angeles, Los Angeles, California 90024

(Received 12 August 1994)

The $\pi N \to \eta N$ and $\eta N \to \eta N$ partial-wave T matrices for the eight lowest partial waves have been obtained in a three-coupled-channel model with unitarity manifestly imposed. The two physical channels are πN and ηN, and the third channel, $\pi\pi N$, is an effective, but unphysical two-body channel which represents all remaining processes. The πN elastic phase shifts and the weighted data base of the $\pi N \to \eta N$ total and differential cross sections are chosen as the input for the fitting procedure. A model containing a single resonance in each of the three partial waves that dominates the η production at lower energies is compared with previous analyses, based on similar assumptions. A multiresonance coupled-channel model is introduced which significantly improves the agreement with all input data. Our results are compared with a complementary multiresonance coupled-channel analysis that is constrained with elastic and continuum production channels. The inclusion of the fourth P_{11} resonance in the 1440–2200 MeV region further improves the agreement between the analysis and the data.

PACS number(s): 25.40.Ve, 13.75.Gx, 14.40.Aq, 24.10.Eq

I. INTRODUCTION

The cross section for η-meson production by pions

$$\pi^- p \to \eta n \tag{1}$$

has a large peak at an energy close to the η production threshold, see Figs. 1(a) and 1(b). The maximum value, $\sigma_{\rm tot}(\pi^- p \to \eta n) = 2.8$ mb, is 6% of $\sigma_{\rm tot}(\pi^- p \to {\rm all})$ [1]. This large peak is usually associated with the $S_{11}(1535)$ isobar known from πN elastic scattering and photoproduction. Recently, Höhler [2] has drawn attention to a peculiar feature of this S_{11} resonance, namely, that the speed plot analysis of S-wave πN scattering has a sharp spike at the opening of the η channel and no clear, independent indication of a resonance in the energy region around 1535 MeV. This suggests a strong interplay between the cusp associated with the opening of the η channel and the excitation of the S_{11} resonance.

Some time ago Bhalerao and Liu [3] analyzed the then available $\pi N \to \eta N$ data in a coupled-channel, single-resonance separable interaction model in which the reaction proceeds via the formation of Δ and N^* isobars and concluded that the S-wave ηN interaction is attractive. They found the value of the S-wave scattering length of $a_{\eta N} = (0.27 + i\,0.22)$ fm. Arima *et al.* [4] obtained $a_{\eta N} = (0.98 + i\,0.37)$ fm, while Wilkin, based on an S-wave threshold enhancement calculation, quotes the value of $a_{\eta N} = (0.55 \pm 0.20 + i\,0.30)$ fm [5]. The large spread in these values of the fundamental $a_{\eta N}$ parameter illustrates the need for better understanding of the ηN system at low energies. The first step to do this is to obtain a reliable set of $\pi N \to \eta N$ T matrices.

The indication of strong and attractive ηN interaction has led to a speculation about the existence of a new type of nuclear matter, namely, quasibound η-mesic nuclei [6]. The properties of this new matter are determined by the ηN interaction at low energies.

Good data on η production in $\pi^- p$ interaction are missing. The dominant contribution to the surprisingly big η production channel is coming from the $S_{11}(1535)$ resonance, the contribution of the $P_{11}(1440)$ and $D_{13}(1520)$ resonances is important, but not completely clarified. The role of other resonances, even in these partial waves, is not at all discussed because of the single-resonance character of the model. Recently, accurate η photoproduction data have been obtained by TAPS at MAMI [7] up to $E_\gamma = 790$ MeV. These data indicate that the D_{13} resonance contribution is small.

The objective of this paper is to furnish a set of $\pi N \to \eta N$ partial-wave T matrices that describe the available data in a straightforward way. It is essential to get reliable information on $\pi N \to \eta N$ on-shell T matrices to be able to calculate the higher-order processes where the η production vertex is a part of the higher-order diagram, for instance in $pp \to pp\eta$. Several publications, dealing with higher-order processes, have either used the dominant S_{11} partial wave [8–10] or have included other partial waves [3, 11] for obtaining the elementary $\pi N \to \eta N$ amplitudes. It is clear from Figs. 1(a) and 1(b), where a comparison of different model predictions with experimental data is given, that only one S-wave resonance is not sufficient, the $S_{11}(1535)$ resonance accounts only for the part of the η production total cross section, for the energy range of the $S_{11}(1535)$ dominance. A single-resonance model for the S wave only is, therefore, incapable of describing all of η production data, but

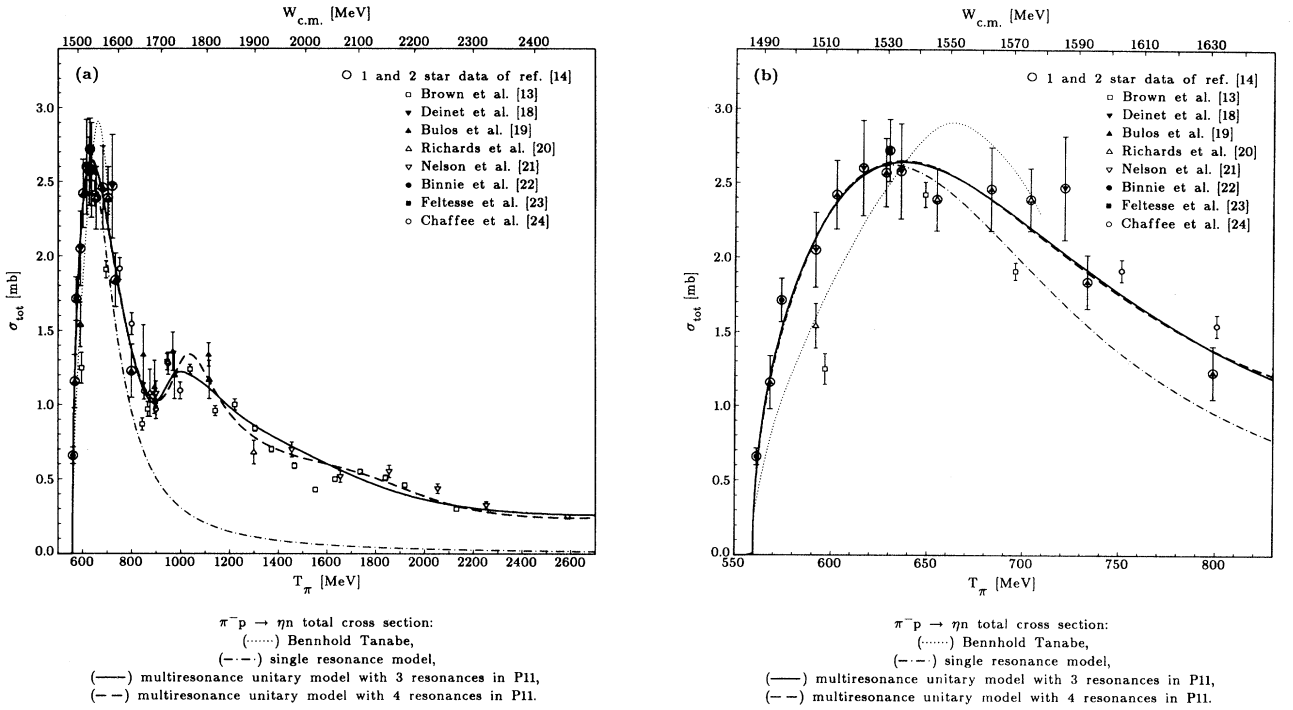

FIG. 1. The total η production cross sections. The experimental data are taken from the literature, as has been indicated in the figure itself. The dotted line is the approximation that only one resonance has a strong branching ratio to the η production channel; the results are taken from [12]. The dash-dotted line is the result of this calculation, and is based on similar assumptions. The full line is the result of the three-coupled-channel multiresonance model presented in this publication with the number of resonances given by the PDG [1], namely three in the P_{11} partial wave. The dashed line is the four P_{11} resonance model. The full lines and the dashed lines show notable difference for the energies above $T_\pi \geq 800$ MeV. The four resonance model for P_{11} is closer to experimental data. (a) is the entire energy range available. (b) is the same data, with an expanded scale for T_π up to 800 MeV.

it may suffice for the region of the $S_{11}(1535)$ dominance, which corresponds to p_π less than 850 MeV/c. To set the stage, we have tested a simple single-resonance model for all three dominant partial waves: S_{11}, P_{11}, and D_{13} without any background terms added. The model describes the large near-threshold peak, but it fails miserably in comparison with data above $T_\pi = 800$ MeV. The recent single-resonance model by Bennhold and Tanabe (BT) [12] is, anyhow, limited to T_π less than 700 MeV. It describes the dominant peak pretty well on the gross scale, but significantly fails in giving details like the exact peak position, etc. [see Fig. 1(b)]. The reason for the failure is that the BT analysis relies on the data of Ref. [13], which suffer from a serious beam momentum calibration error [14]. We have also used data of Ref. [13], but with caution, as elaborated in detail later in the text. The comparison between the two models is shown in Fig. 1(a) and in the expanded scale in Fig. 1(b). Considering that the model of BT [12] used erroneous data of Ref. [13] and has an energy dependent form factor, which is not included in our study, the agreement between the predictions of our single-resonance model and the BT model is satisfactory. Of course, both single-resonance models miserably fail to fit the data above 800 MeV.

To obtain a better description of the input data we propose a multiresonance coupled-channel model with a smooth background added in a unitary way [15] similar as in the Karlsruhe-Helsinki partial-wave analysis (KH PWA) of πN elastic scattering [16]. A data base consisting of πN KH PWA of Ref. [16], with the addition of total and differential $\pi N \to \eta N$ cross sections [1, 13, 17–23] has been chosen in order to perform the fitting procedure of the πN elastic partial waves up to $T_\pi = 2727$ MeV with the additional weighting factors based on the analyses of the data reliability by Clajus and Nefkens [14]. Results for the obtained resonance parameters slightly deviate from the πN elastic case, but they give acceptable $\pi N \to \eta N$ partial-wave T matrices and at the same time predict the T matrices for the ηN elastic process. Manley and Salesky (MS) [24] have used a multichannel and multiresonance K-matrix approach to the coupled-channel inelastic πN scattering with the main inelastic channel being the continuum production. The η production process is only added in two partial waves, the S_{11} and F_{17}. The only purpose for including the η production channel is to maintain unitarity when the observed loss of flux cannot be attributed to any other process. The so-called "η production channel" has to account for *all*

missing inelasticity within the partial wave and cannot be related just to η production. Therefore, the prediction for the two η production partial-wave T matrices S_{11} and F_{17}, which come from the MS model [24, 25], should be used with care. As the complete study of the η production process requires all partial waves we have made a multiresonance three-coupled-channel fit with the ηN channel explicitly included and used as a constraint. The multiresonance MS model [24, 25] is complementary to ours in the sense that our results for the resonance branching ratios for the $\pi^2 N$ channel can be compared to the continuum production branching ratios in the MS model, and they should (but only roughly) correspond.

II. FORMULATION OF THE MODEL

A. The three-coupled-channel formalism

The $\pi N \to \eta N$ process is given by the invariant amplitude

$$A(W,\cos\theta^*) + \not{q}_\eta B(W,\cos\theta^*)$$

with the standard on-shell partial-wave decomposition of A and B:

$$\begin{aligned} A(W,\cos\theta^*) = \frac{4\pi}{\sqrt{q_\pi^{*3} q_\eta^{*3}}} \Bigg\{ & \sum_{l=0}^{\infty} T_{l+} \Big[\sqrt{(E_i^*+m)(E_f^*+m)}(W-m)P_l'(\cos\theta^*) \\ & + \sqrt{(E_i^*-m)(E_f^*-m)}(W+m)P_{l+1}'(\cos\theta^*) \Big] \\ & - \sum_{l=1}^{\infty} T_{l-} \Big[\sqrt{(E_i^*+m)(E_f^*+m)}(W-m)P_{l+1}'(\cos\theta^*) + \sqrt{(E_i^*-m)(E_f^*-m)}(W+m)P_l'(\cos\theta^*) \Big] \Bigg\}, \end{aligned} \tag{2}$$

$$\begin{aligned} B(W,\cos\theta^*) = \frac{4\pi}{\sqrt{q_\pi^{*3} q_\eta^{*3}}} \Bigg\{ & -\sum_{l=0}^{\infty} T_{l+} \Big[\sqrt{(E_i^*+m)(E_f^*+m)}P_l'(\cos\theta^*) - \sqrt{(E_i^*-m)(E_f^*-m)}P_{l+1}'(\cos\theta^*) \Big] \\ & + \sum_{l=1}^{\infty} T_{l-} \Big[\sqrt{(E_i^*+m)(E_f^*+m)}P_{l+1}'(\cos\theta^*) - \sqrt{(E_i^*-m)(E_f^*-m)}P_l'(\cos\theta^*) \Big] \Bigg\}. \end{aligned}$$

W is the total c.m. energy, θ^* is the c.m. scattering angle, q_π^* and q_η^* are the initial pion and final η c.m. momenta, E_i^* and E_f^* are the initial and final nucleon c.m. energies, $P_l'(z)$ are derivatives of Legendre polynomials, $T_{l\pm}$ are the $\pi N \to \eta N$ T matrices, and m is the nucleon mass.

The $\pi N \to \eta N$ T_{l^+,l^-} matrices are matrix elements of the three-channel partial-wave T^{JL} matrix which is given as

$$T^{JL} = \begin{pmatrix} T^{JL}_{\pi\pi} & T^{JL}_{\pi\eta} & T^{JL}_{\pi\pi^2} \\ T^{JL}_{\eta\pi} & T^{JL}_{\eta\eta} & T^{JL}_{\eta\pi^2} \\ T^{JL}_{\pi^2\pi} & T^{JL}_{\pi^2\eta} & T^{JL}_{\pi^2\pi^2} \end{pmatrix},$$

where various channels are denoted by the index π for πN, η for ηN, and π^2 for all other channels ($\pi\Delta$, ρN, $\pi\pi N$, ...). The third channel is effectively described as a two-body process $\pi^2 N$ with π^2 being a quasiparticle with a different mass chosen for each partial wave. We have fixed the channel masses, for each partial wave independently.

B. Single-resonance model

The simplest possible model to represent the πN vertex, and which is directly comparable to earlier analyses [3, 11, 12, 26], has been constructed. Only one resonance without any background terms is used to describe each of the three important partial waves S_{11}, P_{11}, and D_{13}.

The elastic T matrix for each resonance is defined as

$$T^{JL}_{cc}(W) = \frac{\Gamma^{JL}_c(W)/2}{M^{JL} - W - i\Gamma^{JL}_{\rm tot}(W)/2}, \quad c = \pi, \eta, \pi^2. \tag{3}$$

The partial widths are given by

$$\Gamma^{JL}_c(W) = \Gamma^{JL}_c(M^{JL}) \times \begin{cases} \left(\frac{q_c}{q^{JL}_{0c}}\right)^{2L+1} & \text{for } q_c < q^{JL}_{0c}, \\ \left(\frac{2q_c}{q_c + q^{JL}_{0c}}\right)^{2L+1} & \text{for } q_c > q^{JL}_{0c}, \end{cases} \tag{4}$$

and q_c is the c.m. momentum of the channel meson c: π, η, or π^2:

$$q_c \equiv q_c(W) = \frac{\sqrt{(W^2 - (m+m_c)^2)\,(W^2 - (m-m_c)^2)}}{2W} \tag{5}$$

for $m_c = m_\pi, m_\eta, m_{\pi^2}$. $q^{JL}_{0c} \equiv q_c(M^{JL})$ is the c.m. momentum of the channel meson c at the resonance mass M^{JL}.

The exception is P_{11} because its mass is below η threshold. For that case we use

$$\Gamma_\eta^{P_{11}}(W) = \begin{cases} 0 & \text{below } \eta N \text{ threshold,} \\ 100\left(\frac{q_\eta}{410}\right)^3 & \text{above } \eta N \text{ threshold.} \end{cases} \quad (6)$$

This definition of partial widths gives the correct threshold behavior for the T matrix. The total widths are given as

$$\Gamma_{\text{tot}}^{JL}(W) = \Gamma_\pi^{JL}(W) + \Gamma_\eta^{JL}(W) + \Gamma_{\pi^2}^{JL}(W). \quad (7)$$

The inelastic T matrix is given by

$$T_{c_1 c_2}^{JL}(W) = \sqrt{T_{c_1}^{JL}(W) T_{c_1}^{JL}(W)}, \quad c_1, c_2 = \pi, \eta, \pi^2, \quad (8)$$

and the T matrix is defined in such a way as to give a unitary S matrix:

$$S = 1 + 2iT, \quad S^\dagger S = S S^\dagger = 1. \quad (9)$$

Reliable branching ratios of various resonances to the η channel unfortunately are not available except for S_{11}. As can be seen from Table I, all values used in our calcula-

TABLE I. Resonance parameters of the single-resonance model.

Resonance	PDG parameters	Used parameters
$S_{11}(1535)$	m = 1520 to 1555	1535
	Γ = 100 to 250	150
	x_π = 0.35 to 0.55	0.40
	x_η = 0.30 to 0.50	0.42
$P_{11}(1440)$	m = 1430 to 1470	1440
	Γ = 250 to 450	250
	x_π = 0.60 to 0.70	0.60
	$x_\eta = 0$	0[a]
$D_{13}(1520)$	m = 1515 to 1530	1520
	Γ = 110 to 135	120
	x_π = 0.50 to 0.60	0.55
	$x_\eta \sim 0.001$	0.0015

[a] $x_\eta = 0$, i.e., $\Gamma_\eta = 0$ is used below, $\Gamma_\eta = 100(\frac{q_\eta}{410})^3$ above the ηN threshold (see text).

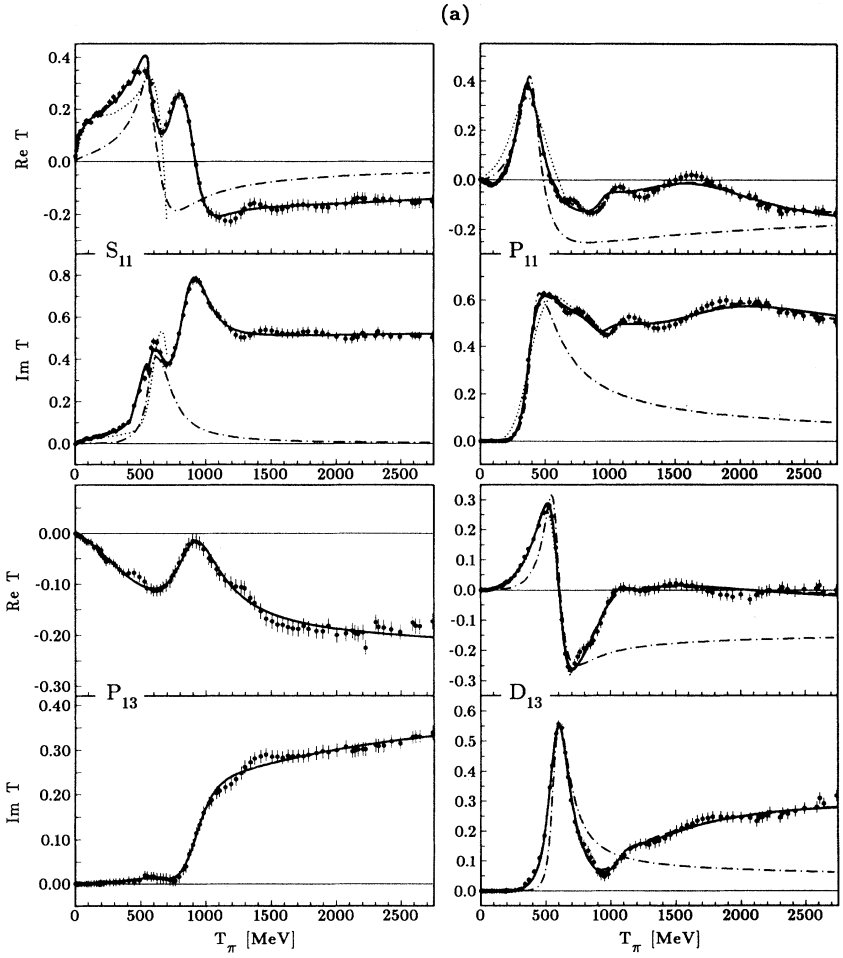

FIG. 2. The πN elastic partial waves. The full circles are the result of the single-channel πN elastic PWA given in Ref. [16]. The used PWA does not give the error analyses for the partial-wave T matrices in [16], so the error bars given in the figure are defined in the text and reflect the statistical weight of the data set used in the minimization procedure. The dotted line is the approximation that only one resonance has a strong branching ratio to the η production channel; the results are from [12]. The dash-dotted line is the result of this calculation, and is based on similar assumptions. The full line is the result of the three-coupled-channel multiresonance model presented here with the number of resonances given by the PDG [1], namely three in the P_{11} partial wave. The dashed line is the four P_{11} resonance model. The full and the dashed lines are practically indistinguishable for all elastic partial waves.

tion are within range of the accepted values [1]. However, the agreement of the elastic πN partial-wave T matrix values with the Karlsruhe-Helsinki phase shift analysis (KH) [16] is not entirely satisfactory for the lower energy range $T_\pi \leq 700$ MeV, and the single-resonance model completely misses all higher-energy partial waves in the elastic channels. The results are shown in Figs. 2(a) and 2(b). The dash-dotted line shows our single-resonance model and the dotted line is the BT single-resonance model of Ref. [12] which has an additional energy dependent form factor. The BT model is limited to lower energies. The dots are the elastic KH πN partial-wave analysis [16]. As the KH PWA does not give the error analysis for the partial-wave T matrices in [16], and the errors are essential to define the statistical weight of the analysis, we have identified the errors of the used data in the standard χ^2 analysis as

$$\Delta_i^{JL} = 0.005 + \left(0.01 + 0.0015\ \frac{W_i - W^{\pi\ \mathrm{thresh}}}{\Delta}\right) |T_{\max}^{JL}|,$$

$\Delta = 1$ GeV.

W_i is the total c.m. energy, $W^{\pi\ \mathrm{thresh}}$ is the total energy at π nucleon threshold, $|T_{\max}^{JL}|$ is the maximal value of the T matrix in the chosen energy range. The energy range extends up to 2.5 GeV of the total c.m. energy. The statistical weight in the χ^2 function is defined in a standard way as well:

$$w_i^{JL} = \frac{1}{(\Delta_i^{JL})^2}.$$

The introduced energy dependence of the statistical weight is inspired by the energy dependence of the error analysis of Ref. [15]. It steadily rises with energy, but does not exceed the value of 0.02 in the units of Ref. [16].

The total cross sections for the η production are compared with the single-resonance model (dash-dotted line) of this article, and the BT single-resonance model of Ref. [12] (dotted line) in Figs. 1(a) and 1(b). The experimental data for the η production differential cross sections are compared with both models in Figs. 3(a)–3(d). The full and dashed lines in Figs. 1–3 will be explained later.

The failure of the single-resonance model to describe

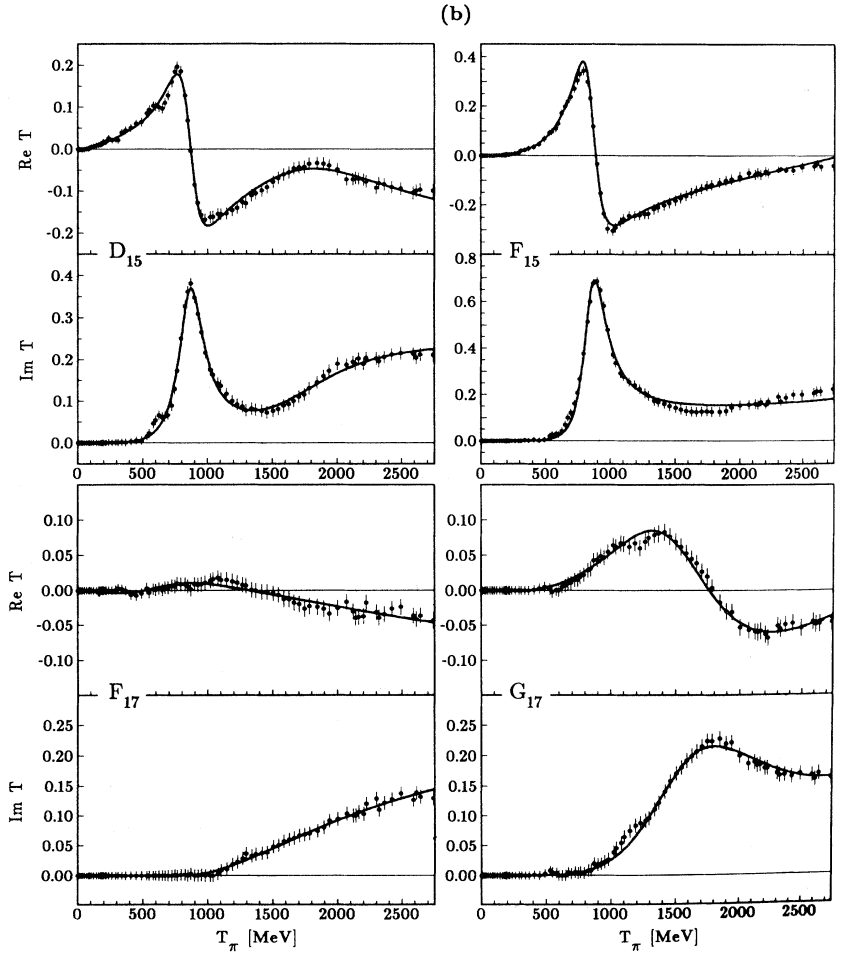

FIG. 2. (*Continued*).

the experimental facts is not unexpected. Even at the lower energies, background terms which are not included in the single-resonance model are of some importance, and their omission can account for the observed discrepancy with the input. The comparison of the parameter-free single-resonance model of this work (dash-dotted line), with the similar BT model [12] (dotted line), shows a fair likeness in the energy range where the latter analysis has been given. The differences between the two models are attributed to the different input data base and to the additional energy dependent form factor used in [12]. However, as is seen in Figs. 1–3, both models show reasonable agreement with the input data for the important πN elastic partial waves S_{11}, P_{11}, and D_{13} at lower energies. Our analysis predicts strong deviations from the fitted πN elastic partial waves at higher energies, for the S_{11} partial wave in particular, so it is to be expected that the results of [12] suffer from a similar disease for higher energies. Similar statements can be and are valid for the total and differential cross sections of η production (Figs. 1 and 3). The phenomenon observed is consistent with the fact that the single-resonance model covers only the energy range of the first peak in $\sigma_{\rm tot}(\pi^- p \to \eta n)$.

Let us mention that in the described single-resonance formalism it is not possible to extrapolate the model to include more than one resonance per partial wave in a straightforward manner without directly violating the S matrix unitarity.

C. A unitary multiresonance model

In order to fit the πN elastic amplitudes of Ref. [16] better than in the single-resonance model we have introduced a manifestly unitary model that enables including more than one resonance and background term per partial wave. It is constructed following the commonly ac-

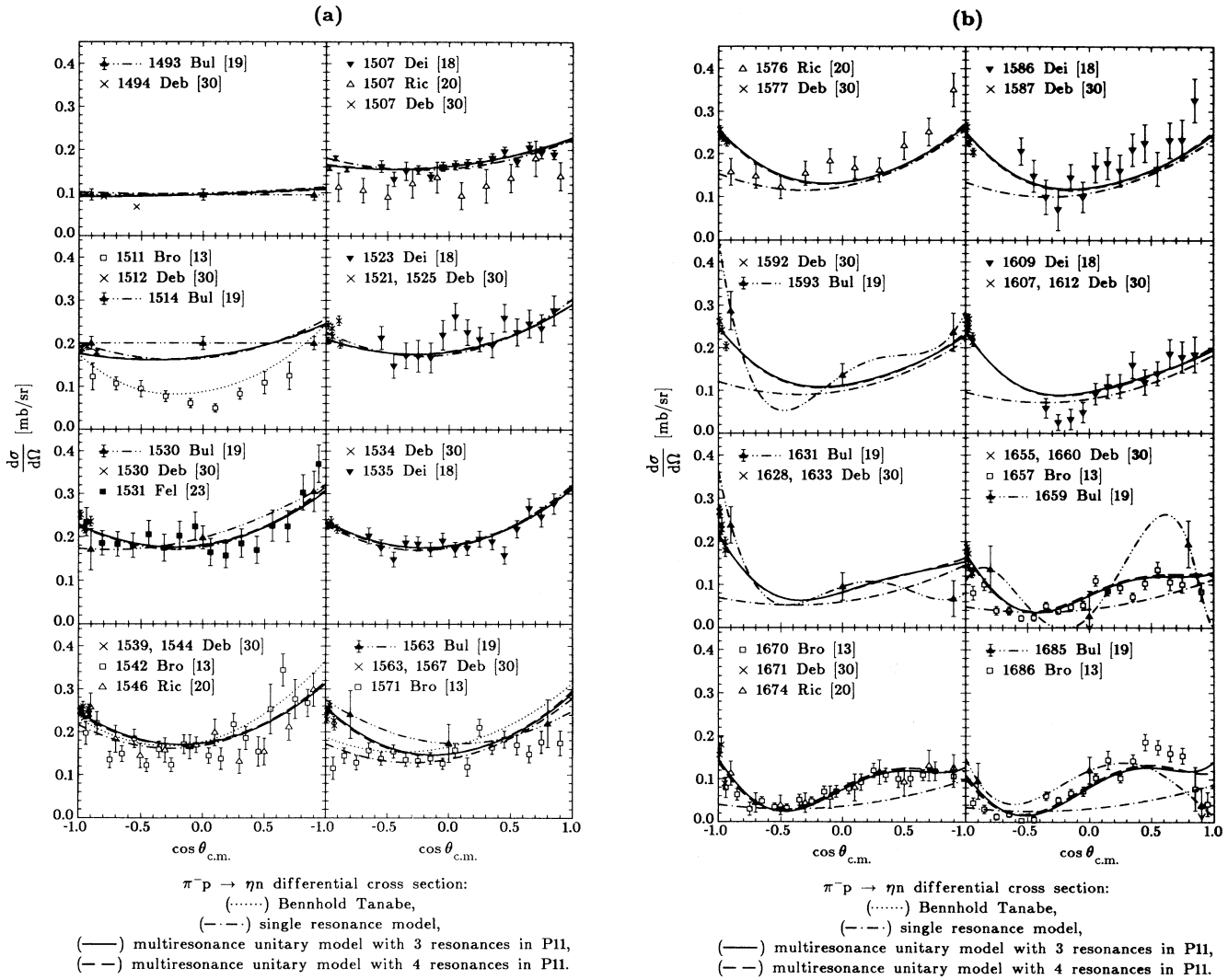

FIG. 3. The comparison of the η production differential cross sections with the aforementioned PWA's. The experimental data taken from the literature are defined in the figure. Curves are as in Fig. 2.

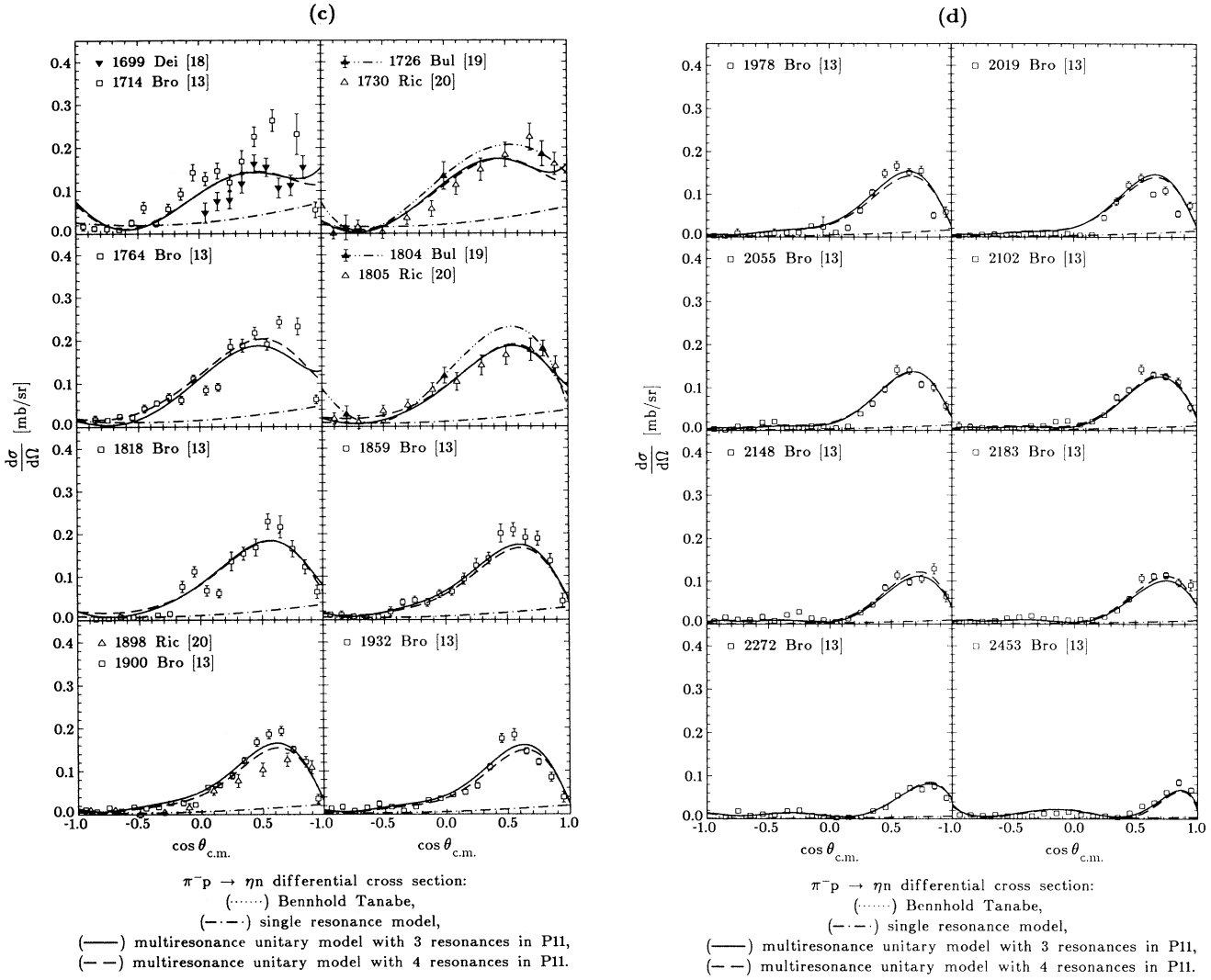

FIG. 3. (*Continued*).

cepted method developed in [15], and originally used in πN elastic partial-wave analysis (PWA) [16].[1]

As the η meson is a pseudoscalar, isospin zero particle, it mixes by isospin violation with the π^0. We have chosen the following three coupled channels to set up the model: the πN, ηN, and a third, an effective two-body channel labeled $\pi^2 N$, which inclusively contains and represents all remaining, even three-body channels ($\pi\Delta$, ρN, $\pi\pi N$, etc.). The objective of the procedure is to simultaneously achieve a good representation of the input πN elastic T matrices, and the experimental η production data (total and differential cross sections) by the values coming out of the model.

We distinguish three basic steps of the presented analysis.

[1]The simple recipe for the modification of the S matrix, which consists of directly adding extra resonances and a smooth background is manifestly nonunitary.

Step 1: Formalism. The multichannel T matrix taken over from [15] is given as

$$T_{ab}^{JL} = \sum_{i,j=1}^{N^{JL}} f_a^{JL}(s)\sqrt{\rho_a}\gamma_{ai}^{JL} G_{ij}^{JL}(s)\gamma_{jb}^{JL}\sqrt{\rho_b} f_b^{JL}(s), \quad (10)$$

$a, b = \pi, \eta, \pi^2$. The initial and final channels couple through intermediate "particles" or resonances labeled with i and j, and

$$f_a^{JL}(s) = \left(\frac{q_a}{Q_{1a} + \sqrt{Q_{2a}^2 + q_a^2}}\right)^L, \quad (11)$$

$$\rho_a(s) = \frac{q_a}{\sqrt{s}}, \quad (12)$$

where $s = W^2$ and q_a is the meson momentum for any of the three channels given as

$$q_a \equiv q_a(W) = \frac{\sqrt{(W^2-(m+m_a)^2)\,(W^2-(m-m_a)^2)}}{2W}. \tag{13}$$

The mass parameter m_{π^2} for the $\pi^2 N$ channel is fixed prior to minimization to the mass value at which the partial wave inelasticities show the opening of the first inelastic channel:

Partial wave	S_{11}	P_{11}	P_{13}	D_{13}	D_{15}	F_{15}	F_{17}	G_{17}
m_{π^2} (MeV)	450	380	370	380	400	370	650	450

γ_{ia}^{JL} are free parameters and are determined by the fitting procedure. For the Q_{1a} and Q_{2a} parameters we choose the values

$$\begin{aligned} Q_{1\pi} &= Q_{2\pi} = m_\pi, \\ Q_{1\eta} &= Q_{2\eta} = m_\eta, \\ Q_{1\pi^2} &= Q_{2\pi^2} = 400 \text{ MeV}. \end{aligned} \tag{14}$$

G_{ij}^{JL} is a dressed propagator for partial wave JL and particles i and j:

$$G_{ij}^{JL}(s) = G_{ij}^{0JL}(s) + \sum_{k,l=1}^{N^{JL}} G_{ik}^{0JL}(s)\Sigma_{kl}^{JL}(s)G_{lj}^{JL}(s). \tag{15}$$

The bare propagator

$$G_{ij}^{0JL}(s) = \frac{e_i\delta_{ij}}{s_i - s} \tag{16}$$

has a pole at the real value s_i. The sign $e_i = \pm 1$ must be chosen to be positive for poles above the elastic threshold which correspond to resonances. The nonresonant background is described by a function that consists of two terms of the form (16) with pole positions below πN threshold. For that case signs of terms are opposite. The positive sign corresponds to the repulsive and the negative sign to the attractive potential. Σ_{kl}^{JL} is the self-energy term for the particle propagator:

$$\Sigma_{kl}^{JL}(s) = \sum_a \gamma_{ka}^{JL}\Phi_a^{JL}(s)\gamma_{la}^{JL}. \tag{17}$$

The imaginary part of $\Phi_a^{JL}(s)$ is the effective phase-space factor for the channel a:

$$\mathrm{Im}\Phi_a^{JL}(s) = \left[f_a^{JL}(s)\right]^2 \rho_a(s) \equiv F_a^{JL}(s). \tag{18}$$

The real part of $\Phi_a^{JL}(s)$ is calculated using a subtracted dispersion relation

$$\Phi_a^{JL}(s) = \frac{s-s_0}{\pi}\int_{s_a}^{\infty} \frac{F_a^{JL}(s')}{(s'-s)(s'-s_0)}ds', \tag{19}$$

where $s_a = (m+m_a)^2$.

The advantage of this approach is that it manifestly maintains the S matrix unitarity for any number of resonance and/or background terms. The disadvantage is that the connection of the parameters γ_{ia}^{JL} and s_i with the conventional resonance parameters M_i^{JL} and Γ_{ia}^{JL} is not direct [15], but has to be calculated.

Step 2: Data base and fitting procedure. The input parameters for the fitting procedure are s_i and γ_{ia} which determine the bare propagator and self-energy term for the particle propagator, see Eqs. (14), (15), and (16), respectively. The parameters Q_{1a} and Q_{2a} which occur in the form factor given in Eq. (10) have been fixed to the mass of the channel a meson. The ones subtracted dispersion relation given in Eq. (19) is solved numerically with the subtraction constant $s_0 = s_a$ and $\Phi_a^{JL}(s_0) = 0$. The stability of the solution has been tested by calculating and reproducing the initial imaginary part, see Eq. (18). The numerical integration has been performed using the adapted Gaussian quadrature method with no significant dependence on the number of points. We should mention that the dispersion relation has been calculated only once, and tabulated for further use to save the CPU because the parameters which form the integrand are not varied in the minimization procedure.

Data base: As the input data to the minimization procedure we have used (1) the KH partial-wave πN analysis [16], (2) total cross sections for the $\pi N \to \eta N$ process [13, 17–23, 28], (3) differential cross sections for the $\pi N \to \eta N$ process [13, 17–20, 22, 23, 28]. We have fitted the πN elastic T matrices for eight $I = 1/2$ partial waves: S_{11}, P_{11}, P_{13}, D_{13}, D_{15}, F_{15}, F_{17}, and G_{17} using the phase shift analysis KH [16] at 90 energies from threshold to 2.5 GeV of the total c.m. energy. We have also tested the use of (CMU-LBL) πN elastic partial wave analyses [15] without any notable differences. At the inception of this work the only PWA that covered the high energy was KH [16]. Since then the VPI group [27] has extended its analysis approximately to 2.1 GeV. We do not anticipate that the use of VPI PWA would introduce any substantial changes into the conclusions coming out of the present analysis. Anyhow, a new analysis based on the VPI PWA is planned to be the subject of a future research. Finally, let us comment that we should have used the total set of experimental data for πN elastic processes instead of limiting the input to the model dependent information coming from PWA's. However, we have assumed that existing PWA's represent the data adequately enough so we can avoid an enormous CPU time consumption.

The data for the second, ηN channel, are the $\pi N \to \eta N$ differential cross sections at 81 energies and total ηN production cross sections at 67 energies [13, 17–23, 28]. The statistical weights of the ηN data, used in the minimization procedure, have been based on the analysis of the world data give in Ref. [14]. In some cases the published statistical weight had to be modified. Problems of consistency among different measurements have been extensively discussed in [14], and the discrepancy for the lower energies of η production differential cross section of data of Ref. [13] has been claimed. It has been argued in Ref. [14] the data of Ref. [13] are systematically too low, and that it is due to an error in the beam momen-

tum calibration which makes the data at lower energies essentially unusable even if one tries to correct them by a momentum shift. The direct reason for that is a strong momentum dependence of the lab $\Leftrightarrow$ c.m. transformation Jacobian. However, at higher energies, it is safe just to perform a 4% momentum shift downward. Therefore, the systematic error, in addition to the published, statistical one, has been added to the questionable data sets reducing their statistical impact. The statistical weight of all differential cross sections of Ref. [13] has been reduced by the factor of 2. In addition, the statistical weight at lowest energies of $W = 1511$ MeV, 1542 MeV, and 1571 MeV has been even more reduced so that their importance in the analysis is practically eliminated.

A systematic error of 0.01 mb/sr has been added to *all* η production differential cross sections. We have decided to do so because of the fact that the quoted errors in all measurements have been of statistical origin only, so most of the errors have been unrealistically low.

The data taken at the energy of 1507 MeV in Ref. [19] as well tend to be too low when the total cross section is calculated [14] and compared to the "world trend." Therefore, the additional systematic error of 0.04 mb/sr has been added to these data.

For similar general reasons the systematic error of 0.02 mb/sr has been added to all the data of Ref. [28].

All "two-star" cross sections, as given in Ref. [14], are taken with the increased statistical factor of 10, while the statistical factor of the remaining cross section data is kept to be 1.

The direct consequence of our choice of the data base statistical weights is seen in Fig. 3(a): Ref. [12] reproduces the data set of Ref. [13] at lower energies (W = 1511, 1546, and 1571 MeV) while our result tends to reproduce other sets much better. Additional, precise measurements for that process are needed in order to eliminate the present uncertainties.

Fitting procedure: We have fitted the eight above-listed lowest $I = 1/2$ partial waves in the following manner.

(a) The number of resonances and the shape of the background is determined by the choice of bare propagator and self-energy term parameters. We have decided to start from the number of resonances in each partial wave as given in [1, 16]; the background is represented by two resonant functions with the constraint that the pole position is far outside the physical region. Only one resonance in the P_{13} and F_{15} partial waves has been used in our analysis, higher (uncertain) resonances have been dropped. The existence of the second P_{13} resonance has been recently suggested, and it was used in the MS πN analyses [24, 25].

(b) In general, we need up to two background terms. They have been numerically represented as tails of resonances having their pole positions far outside the analyzed energy range.[2]

[2]More than one background term was needed in order to obtain some nontrivial, but smooth energy dependent behavior of the background terms.

(c) Error analysis for resonance parameters has been done on the basis of MINUIT, imposing the confidence level of 70% [29].

We have used a standard MINUIT program using as much as 132 parameters in the final run.

The minimization has been complicated, and a lot of technical tricks had to be used to avoid occurrence of local minima which are hard to handle for a minimization with such a number of parameters.

The result of the fitting procedure gives us a full three-channel T matrix, with submatrices describing the $\pi N \to \eta N$ and $\eta N \to \eta N$ processes.

Step 3: Resonance parameters. The pole positions, resonance masses, and widths have to be obtained numerically from the full partial-wave T matrix, following directly the technique developed in [15]. For the convenience of the reader we shall briefly reproduce the essential steps, angular momentum indexes are suppressed.

The poles of the T matrix given in Eq. (10) are found solving the following equation:

$$\det G^{-1} = 0. \tag{20}$$

The eigenvector of the matrix $H \equiv G^{-1}$ has been found at the pole position $s_{\rm pole}$:

$$\sum_j H_{ij}(s_{\rm pole})\chi_j = 0\,. \tag{21}$$

We have defined quantities

$$\eta_c = \sum_i \gamma_{ic}\chi_i \tag{22}$$

which define the coupling of resonance i to the channel c. We consider the width to be an energy dependent quantity involving the phase-space factors

$$\Gamma \sim \sum_c y_c F_c(s),$$
$$y_c = |\eta_c|^2. \tag{23}$$

Near the resonance we parametrize the T matrix as

$$T_{ab} = (B_{ab} - \delta_{ab})/2i + \sum_{cd} B_{ac}^{1/2} F_c^{1/2} \eta_c D^{-1} \eta_d F_d^{1/2} B_{db}^{1/2}, \tag{24}$$

where B_{ab} is a background S matrix and the generalized Breit-Wigner denominator is

$$D(s) = r - s - c\sum_c y_c \Phi_c(s). \tag{25}$$

The real constants r and c are chosen so that $D(s_{\rm pole}) = 0$. The resonance mass, width, and the branching ratios are defined as

$$\begin{aligned} &\mathrm{Re}\ D(M^2) = 0, \\ &\Gamma = \frac{\mathrm{Im}D(M^2)}{M\mathrm{Re}D'(M^2)}, \\ &\Gamma_c = \frac{y_c F_c(M^2)\Gamma}{\sum_a y_a F_a(M^2)} \equiv x_c\Gamma, \end{aligned} \tag{26}$$

TABLE II. Resonance parameters of the multiresonance model with three P_{11} resonances. The results of elastic πN analyses [1, 16, 15] are given in the first column. The results of the partial-wave analysis of this work, as well as results of the PWA of Ref. [24] are given in columns 2–10. NF indicates not found.

States	This publication					Manley *et al.*				
$L_{2I,2J}$	Mass	Width	x_π	x_η	x_{π^2}	Mass	Width	x_π	x_η	x_{π^2}
$(^{x_{el}}_{mass/width})$	(MeV)	(MeV)	(%)	(%)	(%)	(MeV)	(MeV)	(%)	(%)	(%)
$S_{11}(^{38}_{1535/120})$	1543(6)	155(16)	34(9)	63(7)	3(3)	1534(7)	151(21)	51(5)	43(6)	6(3)
$S_{11}(^{61}_{1650/180})$	1668(17)	209(32)	95(6)	5(5)	0.1(1)	1659(9)	173(12)	89(7)	3(5)	8(3)
$S_{11}(^{9}_{2090/95})$	1703(27)	267(53)	52(23)	2(3)	46(21)	1928(59)	414(157)	10(10)	0(3)	90(10)
$P_{11}(^{51}_{1440/135})$	1426(25)	287(53)	61(9)	0(0)	39(9)	1462(10)	391(34)	69(3)	-	31(3)
$P_{11}(^{12}_{1710/120})$	1724(35)	116(47)	5(5)	89(7)	6(5)	1717(28)	478(226)	9(4)	-	55(11)[a]
$P_{11}(^{9}_{2100/200})$	2175(89)	659(207)	9(4)	89(3)	2(2)	1885(30)	113(44)	15(6)	-	83(8)[a]
$P_{13}(^{14}_{1720/190})$	1711(26)	235(50)	18(4)	0.4(1)	82(4)	1717(31)	383(179)	13(5)	-	87(5)
P_{13}	-	-	-	-	-	1879(17)	498(78)	26(6)	-	74(6)
$D_{13}(^{54}_{1520/114})$	1523(16)	141(30)	48(5)	0.1(0.2)	52(5)	1524(4)	124(8)	59(3)	-	41(3)
$D_{13}(^{8}_{1700/110})$	1795(39)	158(46)	6(8)	13(7)	81(11)	1737(44)	249(218)	1(2)	-	99(2)
$D_{13}(^{6}_{2080/265})$	1988(62)	922(191)	12(3)	7(3)	81(3)	1804(55)	447(40)	23(3)	-	77(3)
$D_{15}(^{38}_{1675/120})$	1683(18)	141(22)	31(6)	0.1(0.2)	69(6)	1676(2)	159(7)	47(2)	-	53(2)
$D_{15}(^{7}_{2100/310})$	2237(64)	764(137)	8(4)	0.3(1)	92(4)	-	-	-	-	-
$F_{15}(^{65}_{1680/128})$	1674(12)	126(20)	69(4)	1(0.4)	30(4)	1684(4)	139(8)	70(3)	-	30(3)
$F_{15}(^{4}_{2000/95})$	-	-	-	-	-	1903(87)	494(308)	8(5)	-	92(5)
$F_{17}(^{4}_{1990/35})$	NF	NF	NF	NF	NF	2086(28)	535(115)	6(2)	94(2)	-
$G_{17}(^{14}_{2190/390})$	2202(67)	807(140)	19(5)	0.1(1)	81(5)	2127(9)	547(48)	22(1)	-	78(1)

[a]Missing inelasticity is going to $K\Lambda$ channel.

where D' is the derivative of the generalized Breit-Wigner denominator (25). The obtained resonance parameter values are given in Tables II and III.

III. RESULTS OF THE UNITARY MULTIRESONANCE MODEL WITH THREE P_{11} RESONANCES

We have obtained the partial-wave T matrices for πN elastic scattering [see Figs. 2(a) and 2(b)], $\pi N \to \eta N$ [see Figs. 4(a) and 4(b)] and ηN elastic scattering [see Figs. 5(a) and 5(b)], on the basis of our fit to the πN elastic and $\pi N \to \eta N$ data. The agreement with the input πN elastic KH PWA T matrices is given in Fig. 2, while the agreement with the input $\pi N \to \eta N$ differential cross sections is given in Fig. 3. The full, dash-dotted, and dotted lines systematically denote the results of our multiresonance, and the two single-resonance models, this publication, and BT, respectively. The T matrix for ηN

TABLE III. Resonance parameters of the multiresonance model with four P_{11} resonances. NF indicates not found.

States	This publication					Manley *et al.*				
$L_{2I,2J}$	Mass	Width	x_π	x_η	x_{π^2}	Mass	Width	x_π	x_η	x_{π^2}
$(^{x_{el}}_{mass/width})$	(MeV)	(MeV)	(%)	(%)	(%)	(MeV)	(MeV)	(%)	(%)	(%)
$S_{11}(^{38}_{1535/120})$	1543(6)	155(16)	34(9)	63(7)	3(3)	1534(7)	151(21)	51(5)	43(6)	6(3)
$S_{11}(^{61}_{1650/180})$	1668(16)	208(31)	94(8)	6(5)	0.2(3)	1659(9)	173(12)	89(7)	3(5)	8(3)
$S_{11}(^{9}_{2090/95})$	1705(27)	271(53)	51(22)	1(3)	48(21)	1928(59)	414(157)	10(10)	0(3)	90(10)
$P_{11}(^{51}_{1440/135})$	1420(18)	246(60)	56(7)	0(0)	44(7)	1462(10)	391(34)	69(3)	-	31(3)
$P_{11}(^{12}_{1710/120})$	1754(32)	180(58)	7(16)	15(11)	78(25)	1717(28)	478(226)	9(4)	-	55(11)[a]
P_{11}	1750(28)	111(36)	11(26)	4(9)	85(22)	1885(30)	113(44)	15(6)	-	83(8)[a]
$P_{11}(^{9}_{2100/200})$	2215(70)	449(175)	11(7)	86(6)	3(4)	-	-	-	-	-
$P_{13}(^{14}_{1720/190})$	1711(26)	235(51)	18(4)	1(2)	81(5)	1717(31)	383(179)	13(5)	-	87(5)
P_{13}	-	-	-	-	-	1879(17)	498(78)	26(6)	-	74(6)
$D_{13}(^{54}_{1520/114})$	1527(18)	142(30)	46(6)	0.2(0.2)	54(6)	1524(4)	124(8)	59(3)	-	41(3)
$D_{13}(^{8}_{1700/110})$	1797(48)	240(62)	4(5)	11(6)	85(9)	1737(44)	249(218)	1(2)	-	99(2)
$D_{13}(^{6}_{2080/265})$	2013(76)	1153(228)	8(2)	8(4)	84(3)	1804(55)	447(40)	23(3)	-	77(3)
$D_{15}(^{38}_{1675/120})$	1683(19)	142(23)	31(6)	0.1(0.1)	69(6)	1676(2)	159(7)	47(2)	-	53(2)
$D_{15}(^{7}_{2100/310})$	2237(65)	755(138)	8(4)	0.2(1)	92(4)	-	-	-	-	-
$F_{15}(^{65}_{1680/128})$	1674(12)	125(20)	70(4)	0.4(0.4)	30(4)	1684(4)	139(8)	70(3)	-	30(3)
$F_{15}(^{4}_{2000/95})$	-	-	-	-	-	1903(87)	494(308)	8(5)	-	92(5)
$F_{17}(^{4}_{1990/35})$	NF	NF	NF	NF	NF	2086(28)	535(115)	6(2)	94(2)	-
$G_{17}(^{14}_{2190/390})$	2198(69)	808(143)	19(5)	0.1(1)	81(5)	2127(9)	547(48)	22(1)	-	78(1)

[a]Missing inelasticity is going to $K\Lambda$ channel.

elastic scattering is a prediction. All observables, obtainable on the basis of our results for the partial-wave T matrix of the $\pi N \to \eta N$ and ηN elastic reactions, with the exception of the $\pi N \to \eta N$ differential cross sections, which are input data, are henceforth a prediction. Our T matrices can be used as input to η production calculations in reactions such as $pp \to pp\eta$.

As can be seen, single-resonance models give a reasonable agreement only in the region of the $S_{11}(1535)$. They can be used for higher-order calculations, only for a limited energy range where one resonance per partial wave dominates. However, the analysis presented in this work, which is based on more than one resonance per partial wave, can be used over the full energy range.

The results of the multiresonance model for the πN interaction by MS [24] can be used as a consistency check. The parameters of both models, for the same number of resonances per partial wave (those given by the PDG [1]) are listed in Table II. We may call these analysis complementary because the inelastic part of the πN partial waves is constrained by two complementary processes: η production in our case, and continuum production in the case of Ref. [24]. Therefore, the π^2 part of our analysis should roughly correspond to the $\pi\pi$ part of another analysis, and the parameters of the η production partial waves explicitly included in other analysis should correspond to our findings. Of course, masses and widths of resonances should correspond to the values given by the KH and CMU-LBL πN elastic analyses, which are generally accepted by the Particle Data Group (PDG) [1].

As can be seen from Figs. 1–3, the multiresonance model, based on the standard number of resonances, describes, the input $\pi N \to \pi N$ and $\pi N \to \eta N$ data fairly well. Of course, the η production cross sections are as well correctly described in the full energy range. The structure of the πN elastic partial waves [16] is not entirely reproduced. The tendency of smoothing elastic partial waves, as has been already indicated previously, exists when the inelastic channels are explicitly included. Therefore, we are tempted to conclude that inclusion of inelastic processes imposes some restrictions on the elastic channel, forcing partial waves to have less structure than in [16].

Comparing the available analyses we conclude the fol-

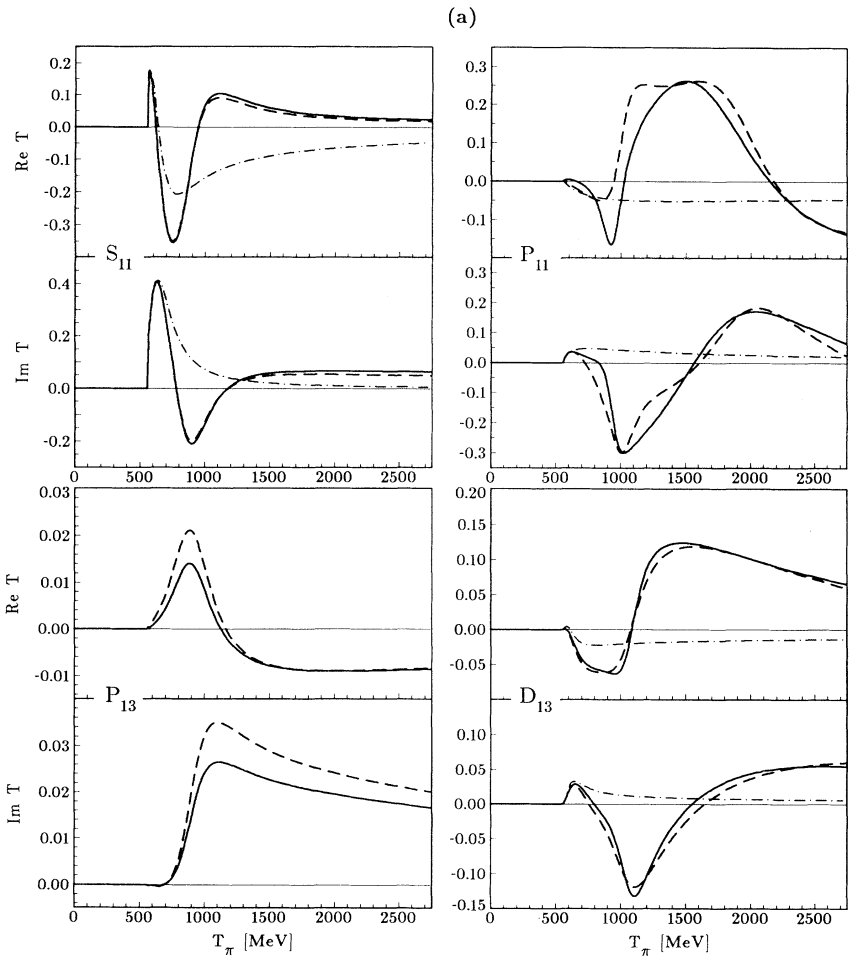

FIG. 4. The partial-wave T matrix for the η production channel. The dash-dotted line is the single-resonance approximation for S_{11}, P_{11}, and D_{13} partial waves of this work. The full line is the result of the three-coupled-channel multiresonance model presented here, with the number of resonances given by the PDG [1], namely three in the P_{11} partial wave. The long-dashed line represents the increase to four resonances in the P_{11} partial wave. Differences between long-dashed and full lines are quite notable in this figure.

lowing.

(1) The masses and πN elastic branching ratios generally agree for all three PWA's, with the exception of the P_{11}. This problem is discussed later.

(2) All partial waves *except* the P_{11} show reasonable agreement in both multichannel models.

(3) The two higher P_{11} partial-wave resonances of MS and our analyses do not agree. The branching ratio for η production in our model is about 90%. The MS model [24] predicts almost a 60% branching ratio to the $\pi\pi$ channel, leaving no freedom for any flux going to the η production channel. The disagreement is obvious, and we shall offer a natural explanation.

IV. RESULTS OF THE UNITARY MULTIRESONANCE MODEL WITH FOUR P_{11} RESONANCES

Inspection of the resonance parameters of Ref. [24] reveals the following (see Table II): the total width of the $P_{11}(^{51}_{1440/135})$ is different from the ones of KH [16], CMU-LBL [15], and Arndt *et al.* [27]; the total width of the $P_{11}(^{12}_{1710/120})$ is different from the ones of KH [16], CMU-LBL [15], and Arndt *et al.* [27]; the mass of the $P_{11}(^{9}_{2100/200})$ is much lower than the ones of KH [16] and CMU-LBL [15]; the mass of the $D_{13}(^{6}_{2080/265})$ is shifted from 2080 to 1804 MeV. Therefore, we suspect that a part of the physics in the vicinity of the 1800 MeV mass region is not entirely taken into account.

We assume that there is another degree of freedom in the P_{11} partial wave, in the form of another resonance.

This possibility of having four instead of three resonances in the P_{11} channel leads to a fit which is shown in the figures with dashed lines. The resonance parameters are given in Table III. The T-matrix pole positions for KH [16], CMU-LBL[15], MS [24], and our analyses (three and four poles) are given in Fig. 6.[3] As can be seen in Fig. 6, the pole positions of the three resonances are well established in the classical πN elastic PWA's and are fairly close. The P_{11} T-matrix pole positions for the

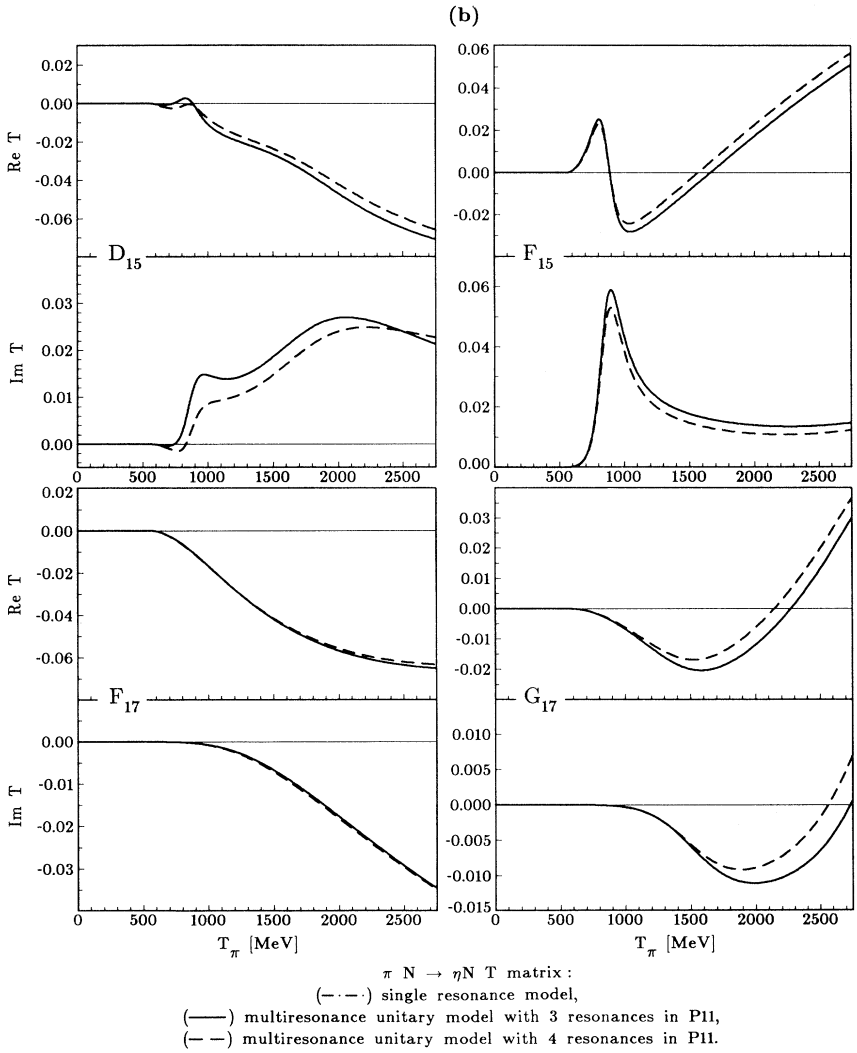

FIG. 4. (*Continued*).

[3]CMU-LBL and our analyses give the exact T-matrix pole positions, while the poles for the remaining analyses have been approximated by $M - i\Gamma/2$.

MS analysis [24] (given by full circles) are quite different from the recommended values. The three-pole version of the P_{11} of our calculation is also quite compatible with the KH and CMU-LBL pole positions. The four-pole version of the P_{11} shows agreement for the lowest pole, the next two poles are near in masses, but distinctly separated in the complex energy plane, while the fourth pole is somewhat lower than KH. In our analysis the fourth resonance is strongly inelastic, going mainly to the η production channel, therefore it is not to be expected that either of the KH or MS analyses could determine it with great precision.

V. CONCLUSIONS

(1) The addition of another resonance in the P_{11} partial wave definitely improves our fit to elastic and inelastic data in all channels. Various quark models also predict four and even five P_{11} resonances in the energy region of 1440–2200 MeV [30, 31].

(2) The changes in πN elastic partial waves are negligible because all the resonances (with the exception of the first one) are strongly inelastic.

(3) The changes in η production and ηN elastic channel T matrices are clearly visible in all partial waves. As is to be expected, the P_{11} is significantly changed, while other partial waves do show some variation. However, let us draw the reader's attention to the fact that S_{11}, P_{11}, and D_{13} partial waves are the dominant ones, while the contribution of other channels is at least the order of magnitude lower. So, even if the relative change in Figs. 4 and 5 is large for other partial waves, the change at the absolute scale is comparably small.

(4) The inconsistency problem between the two inelastic PWA's goes away. The two P_{11} resonances in the vicinity of 1750 MeV are responsible for the continuum production; this is to be compared with 1717 and 1885 resonances of Ref. [24], the third resonance at 2215 almost completely couples to the ηN channel, with a very small branching ratio to the continuum production.

(5) The MS PWA [24] could not easily see the additional fourth P_{11} resonance as it mostly couples to the η production channel, and it is not, in their case, explicitly included.

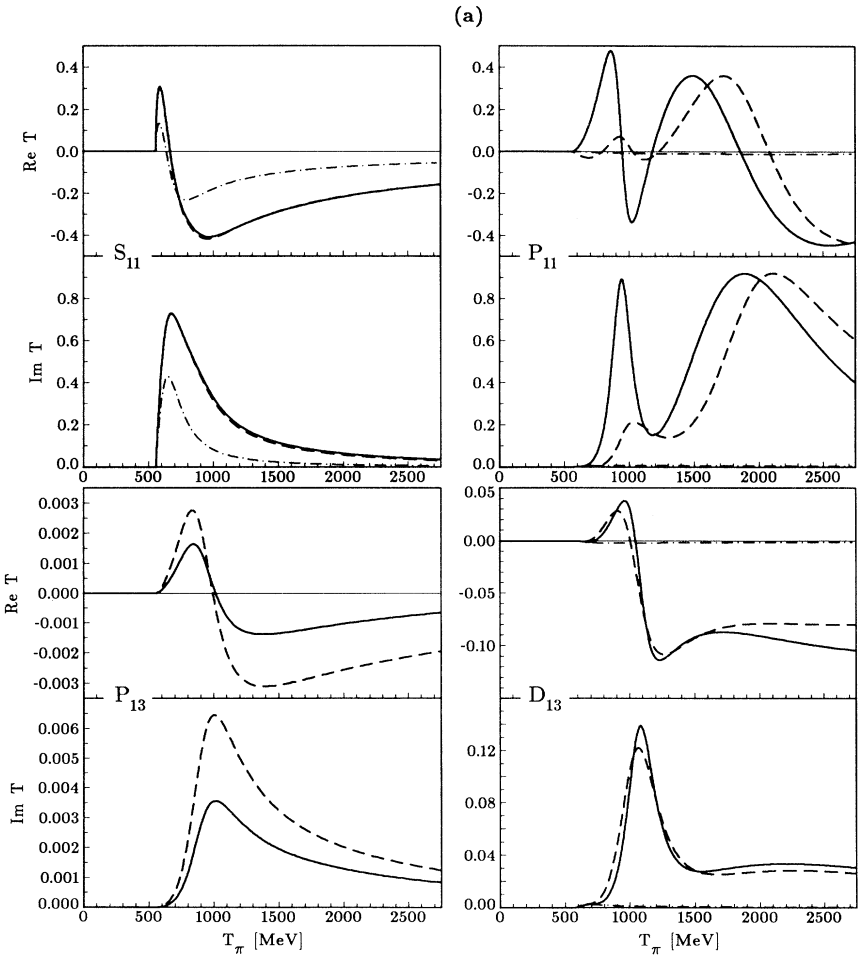

FIG. 5. The partial-wave T matrix for the ηN elastic channel. Differences between dashed (four P_{11} resonances) and full lines (three P_{11} resonances) are quite pronounced.

TABLE IV. Resonance parameters of the multiresonance models with three P_{11} and four P_{11} resonances using the data of Ref. [13], for $T_\pi > 900$ MeV shifted downward by 30 MeV. Brown data below 900 MeV are omitted from fitting procedure. NF indicates not found.

States	Three-resonance model					Four-resonance model				
$L_{2I,2J}$ ($^{x_{el}}_{mass/width}$)	Mass (MeV)	Width (MeV)	x_π (%)	x_η (%)	x_{π^2} (%)	Mass (MeV)	Width (MeV)	x_π (%)	x_η (%)	x_{π^2} (%)
$S_{11}(^{38}_{1535/120})$	1542(6)	152(15)	34(8)	63(7)	3(3)	1542(6)	150(15)	34(9)	63(7)	3(3)
$S_{11}(^{61}_{1650/180})$	1669(17)	212(32)	95(6)	5(5)	0.1(2)	1669(17)	215(32)	94(7)	6(5)	0.2(2)
$S_{11}(^{9}_{2090/95})$	1709(27)	270(52)	51(22)	2(4)	47(20)	1713(27)	279(54)	49(21)	2(3)	49(19)
$P_{11}(^{51}_{1440/135})$	1426(25)	286(95)	61(9)	0(0)	39(9)	1421(18)	250(63)	56(8)	0(0)	44(8)
$P_{11}(^{12}_{1710/120})$	1722(37)	114(47)	5(5)	89(7)	6(5)	1766(34)	185(61)	8(14)	16(10)	76(21)
P_{11}	-	-	-	-	-	1760(29)	109(32)	11(25)	3(7)	86(22)
$P_{11}(^{9}_{2100/200})$	2180(90)	666(209)	9(4)	89(3)	2(2)	2203(70)	418(171)	11(7)	86(7)	3(4)
$P_{13}(^{14}_{1720/190})$	1711(26)	235(50)	18(4)	0.3(1)	82(4)	1711(26)	235(51)	18(4)	0.2(1)	82(4)
P_{13}	-	-	-	-	-	-	-	-	-	-
$D_{13}(^{54}_{1520/114})$	1524(16)	141(30)	48(5)	0.1(0.2)	52(5)	1526(18)	143(32)	46(6)	0.1(0.2)	54(6)
$D_{13}(^{8}_{1700/110})$	1800(42)	181(51)	6(7)	12(7)	82(10)	1791(46)	215(60)	4(5)	10(6)	86(9)
$D_{13}(^{6}_{2080/265})$	2020(68)	1045(206)	11(3)	7(4)	82(3)	1986(75)	1050(225)	9(2)	7(4)	84(3)
$D_{15}(^{38}_{1675/120})$	1683(18)	142(22)	31(6)	0.1(0.3)	69(6)	1683(19)	142(23)	31(6)	0.1(0.1)	69(6)
$D_{15}(^{7}_{2100/310})$	2238(64)	769(138)	8(4)	0.3(1)	92(4)	2240(65)	761(139)	8(4)	0.1(1)	92(4)
$F_{15}(^{65}_{1680/128})$	1674(12)	126(20)	70(4)	0(0.4)	30(4)	1674(12)	126(20)	69(4)	1(0.4)	30(4)
$F_{15}(^{4}_{2000/95})$	-	-	-	-	-	-	-	-	-	-
$F_{17}(^{4}_{1990/35})$	NF	NF	NF	NF	NF	NF	NF	NF	NF	NF
$G_{17}(^{14}_{2190/390})$	2202(66)	807(137)	19(5)	0.1(0.4)	81(5)	2198(68)	805(140)	19(5)	0.1(0.3)	81(5)

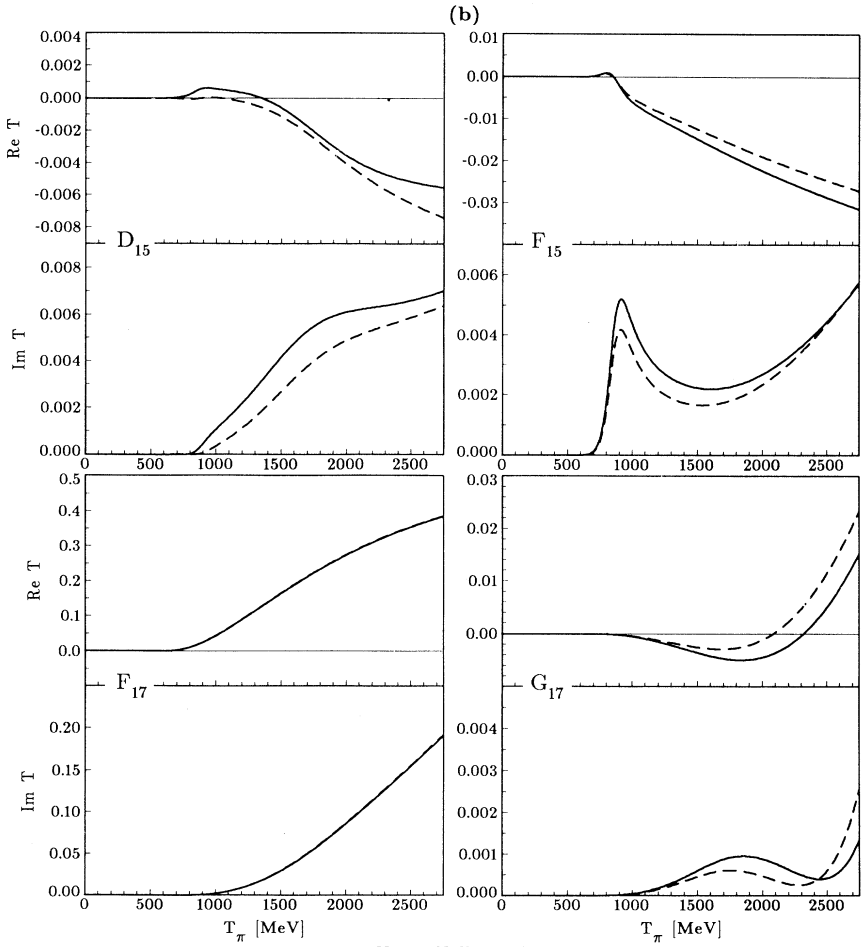

FIG. 5. (*Continued*).

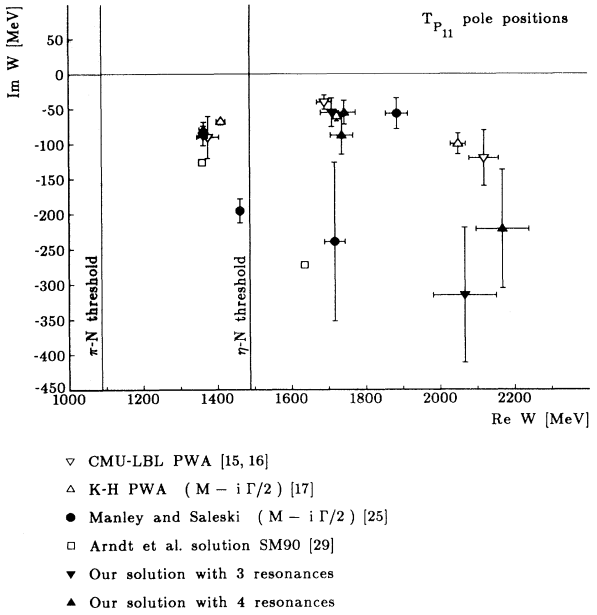

FIG. 6. The pole positions for all four partial-wave analyses mentioned in this work. The notation is given explicitly in the figure.

(6) The elastic πN analyses [15, 16] have problems of determining the number and parameters of the resonances going to inelastic channels. Some changes in the resonances with a small elastic branching ratio should be easy to obtain in the single-channel formalism.

(7) If the Brown data for $T_\pi > 900$ MeV are shifted to lower energies by 30 MeV and data below 900 MeV are omitted then the resonance parameters for our solutions containing 3 and 4 resonances in the P_{11} are shown in Table IV. The results are virtually identical (within errors) with the solutions using all originally published Brown data [13]. That indicates that our PWA is showing robustness with respect to possible errors in input.

Of course, adding an extra P_{11} resonance is only one way of making our analysis compatible to MS PWA; there might be other, equally good explanations of the apparent disagreements when the inelastic branching ratios are compared. One technical detail has to be kept in mind: the background parts are represented by two resonances with poles kept far outside the range of interest. Therefore, the background is also fitted. The proper way should be to calculate the background in some model (for instance a cloudy bag model), to fix it, and then fit just the resonant part [32]. The interference of background and resonant parts might shift the resonance parameters notably.

The T matrices obtained in this study are an essential ingredient for calculating η production reactions $D(\pi, NN)\eta$ and $D(\pi, NN)\pi$. The off-mass-shell extrapolation procedure for the η production amplitudes cannot be determined in this formalism. We do hope to learn something about these effects from the higher-order processes, assuming that the off-mass shell behavior of the η particle is similar as of the pions [33].

This work was partly supported by the EC Contract CI1*-CT-91-0894 and DOE Contract DE-FG03-88ER40420/A606.

[1] Particle Data Group, K. Hikasa *et al.*, Phys. Rev. D **45**, S1 (1992).
[2] G. Höhler, in *πN Newsletter*, edited by G. Höhler, V. Kluge, and B.M.K. Nefkens (University of California, Los Angeles, 1993), No. 9, p. 1.
[3] R.S. Bhalerao and L.C. Liu, Phys. Rev. Lett. **54**, 865 (1985).
[4] M. Arima, K. Shimizu, and K. Yazaki, Nucl. Phys. **A243**, 613 (1993).
[5] C. Wilkin, Phys. Rev. C **47**, 938 (1993).
[6] L.C. Liu and Q. Haider, Phys. Rev. C **34**, 1845 (1986).
[7] B. Krusche, *Proceedings of the I TAPS Workshop*, Alicante, 1993 (World Scientific, Singapore, 1993).
[8] T. Vetter, A. Engel, T. Biro, and U. Mosel, Phys. Lett. B **263**, 153 (1991).
[9] J.M. Laget, F. Wellers, and J.F. Lecolley, Phys. Lett. B **257**, 254 (1991).
[10] R.C. Carrasco, Phys. Rev. C **48**, 2333 (1993).
[11] H.C. Chiang, E. Oset, and L.C. Liu, Phys. Rev. C **44**, 738 (1991).
[12] C. Bennhold and H. Tanabe, Nucl. Phys. **A350**, 625 (1991).
[13] R.M. Brown, A.G. Clark, P.J. Duke, W.M. Evans, R.J. Gray, E.S. Groves, R.J. Ott, H.R. Renshall, A.J. Shah, J.J. Thresher, and M.W. Tyrrell, Nucl. Phys. **B153**, 89 (1979).
[14] M. Clajus and B.M.K. Nefkens, in *πN Newsletter* [2], No. 7, p. 76.
[15] R.E. Cutkosky, R.E. Hendrick, J.W. Alcock, Y.A. Chao, R.G. Lipes, J.C. Sandusky, and R.L. Kelly, Phys. Rev. D **20**, 2804 (1979); R.E. Cutkosky, C.P. Forsyth, R.E. Hendrick, and R.L. Kelly, *ibid.* **20**, 2839 (1979); R.K. Kelly and R.E. Cutkosky, *ibid.* **20**, 2782 (1979).
[16] G. Höhler, in *Elastic and Charge Exchange Scattering of Elementary Particles*, edited by H. Schopper, Landolt-Börnstein, New Series, Group X, Vol. 9, Part 2 (Springer-Verlag, Berlin, 1983).
[17] W. Deinet, H. Müller, D. Schmitt, H.M. Staudenmaier, S. Buniatov, and E. Zavattini, Nucl. Phys. **B11**, 495 (1969).
[18] F. Bulos, R.E. Lanou, A.E. Pifer, A.M. Shapiro, C.A. Bordner, A.E. Brenner, M.E. Law, E.E. Ronat, F.D. Rudnick, K. Strauch, J.J. Szymanski, P. Bastien, B.B. Brabson, Y. Eisenberg, B.T. Feld, V.K. Kistiakowsky, I.A. Pless, L Rosenson, R.K. Yakamoto, G. Calvelli, F. Gasparini, L. Guriero, G.A. Salandin, A. Tomasin, L. Ventura, C. Voci, and F. Waldner, Phys. Rev. **187**, 1827 (1969).
[19] B.W. Richards, C.B. Chiu, R.D. Eandi, C.A. Helmholz, R.W. Kenney, B.J. Moyer, J.A. Poirier, R.J. Cence, V.Z. Peterson, N.K. Sehgal, and V.J. Stenger, Phys. Rev. D **1**, 10 (1970).
[20] J.E. Nelson, Ph.D. thesis, Lawrence Berkeley Laboratory,

1972.
[21] D.M. Binnie *et al.*, Phys. Rev. D **8**, 2793 (1973).
[22] J. Feltesse, R. Ayed, P. Bareyre, P. Borgeaud, M. David, J. Erwein, Y. Lemoigne, and G. Villet, Nucl. Phys. **B93**, 242 (1975).
[23] R.B. Chaffee, Ph.D. thesis, Lawrence Berkeley Laboratory, 1975.
[24] D.M. Manley and E.M. Saleski, Phys. Rev. D **45**, 4002 (1992), and references therein.
[25] D.M. Manley, in πN *Newsletter* [2], Vol. 8, p. 141.
[26] Q. Haider and L.C. Liu, Phys. Lett. B **172**, 257 (1986).
[27] R.A. Arndt, Li Zhujun, L.D. Roper, R.L. Workman, and J.M. Ford, Phys. Rev. D **43**, 2131 (1991).
[28] N.C. Debenham, D.M. Binnie, L. Camilleri, J. Carr, A. Duane, D.A. Garbutt, W.G. Jones, J. Keyne, I. Siotis, and J.G. McEwen, Phys. Rev. D **12**, 2545 (1975).
[29] MINUIT Reference Manual, Ver. 92.1, Application Software Group, CERN Program Library Long Writeup **D506**, 75 (1992).
[30] R. Koniuk and N. Isgur, Phys. Rev. D **21**, 1868 (1980).
[31] S. Capstik and W. Roberts, Phys. Rev. D **49**, 4570 (1994).
[32] T.-S.H. Lee, private communication.
[33] M. Batinić, T.-S.H. Lee, M.P. Locher, Y. Lu, and A. Švarc, unpublished.